EFDA–JET–PR(11)44

H. Weisen, Y. Camenen, A. Salmi, T.W. Versloot, P.C. de Vries,
M. Maslov, T. Tala, M. Beurskens, C. Giroud
and JET EFDA contributors

Identification of the Ubiquitous Coriolis Momentum Pinch in JET Tokamak Plasmas

Identification of the Ubiquitous Coriolis Momentum Pinch in JET Tokamak Plasmas

H. Weisen[1], Y. Camenen[2], A. Salmi[3], T.W. Versloot[4], P.C. de Vries[4], M. Maslov[5], T. Tala[6], M. Beurskens[5], C. Giroud[5] and JET-EFDA contributors*

JET-EFDA, Culham Science Centre, OX14 3DB, Abingdon, UK

[1]Centre de Recherches en Physique des Plasmas, Association EURATOM - Confédération Suisse, EPFL, 1015 Lausanne, Switzerland
[2]IIFS/PIIM UMR 7345/Aix-Marseille Univ., Marseille, France
[3]Association EURATOM-Tekes, Aalto University, Finland
[4]FOM Institute Rijnhuizen, Association EURATOM-FOM, The Netherlands
[5]EURATOM-CCFE Fusion Association, Culham Science Centre, OX14 3DB, Abingdon, OXON, UK
[6]Association EURATOM-Tekes, VTT, Finland
** See annex of F. Romanelli et al, "Overview of JET Results", (23rd IAEA Fusion Energy Conference, Daejon, Republic of Korea (2010)).*

Preprint of Letter to be submitted for publication in
Nuclear Fusion

ABSTRACT.
A broad survey of the experimental database of neutral beam heated plasmas in the JET tokamak has established the theoretically expected ubiquity, in rotating plasmas, of a convective transport mechanism which has its origin in the vertical particle drift resulting from the Coriolis force. This inward convection, or pinch, leads to inward transport of toroidal angular momentum and is characterised by pinch numbers RV/χ_ϕ, which rise from near unity at r/a ≈ 0.25 to around 5 at r/a ≈ 0.85. Linear gyrokinetic calculations of the Coriolis pinch number and the Prandtl number χ_ϕ/χ_i, are in good agreement with the experimental observations, with similar dependencies on plasma parameters. The data, however, do not rule out contributions from different processes, such as residual stresses.

INTRODUCTION
In view of mounting experimental evidence for momentum transport processes that cannot be attributed to diffusion alone [1-7] and theoretical predictions thereof [8-12], a broad survey of recent experiments in the JET tokamak [13] was undertaken to ascertain the ubiquity of non-diffusive processes and their parameter dependencies. Most importantly, this work was to establish whether the observations support the theoretical prediction [8-10] of a convective effect arising in Neutral Beam heated rotating plasmas typical for JET. In a co-rotating frame of reference description [8], this convective effect, named the Coriolis pinch, results from the vertical drift due to the Coriolis force, which generates a momentum flux proportional to the frame rotation, by coupling density and parallel velocity perturbations.

The database constituted for this purpose contains several hundred steady-state profiles measured using standard diagnostics such as Charge eXchange Recombination Spectroscopy (CXRS) for angular velocity and ion temperature and Thomson scattering for electron density and temperature. The data are taken both in the standard high confinement mode (H-mode) and in 'hybrid scenarios' [14], with dominant heating by Neutral Beam Injection (NBI) in the range 5-20MW and operation in deuterium. The H-modes achieved global confinement improvement factors H98 with respect to the IPB98(y,2) global multi-machine scaling [15] in the range 0.6-1, while recent hybrid regimes had H98 factors up to 1.45. Together those two confinement regimes constitute the mainstay of the JET operating domain over recent years and provide two of the main scenarios foreseen for the ITER project [16].

In steady state, the local momentum transport equation is simply given by the balance between the local torque surface density t (N/m) from NBI and the momentum flux:

$$t = -\chi_\phi l \nabla\omega/\omega + \left(\frac{\Gamma_N}{n_i} + V\right) l + \tau_{rs} \qquad (1)$$

Here $l = m_i\, n_i\, R^2 \omega$ is the angular momentum density with m_i the average ion mass, n_i the ion density, R the average major radius of the flux surface under consideration and ω the toroidal

angular velocity. The momentum flux is split into a diffusive part, $-\chi_\phi l \nabla\omega/\omega$, with χ_ϕ the radial momentum diffusivity, a convective part $(\Gamma_N/n_i+V)l$ with V the momentum pinch velocity and Γ_N the particle flux associated with the particle source provided by NBI, and a residual stress part τ_{rs}. The convective part is predicted to be the sum of the contribution of the particle flux and of the theoretically predicted Coriolis pinch [9,10]. Various mechanisms, reviewed in [8], can lead to residual stresses. Eq.(1) is rearranged and normalised such as to express the normalised angular frequency gradient $R/L_\omega = R\nabla\omega/\omega$ as a sum of dimensionless terms associated with diffusion, convection and a residual stress term:

$$R/L_\omega = -\frac{\chi_i}{\chi_\phi}\left\{\frac{Rt}{\chi_i l} - \frac{R\Gamma_N}{\chi_i n_i}\right\} + \frac{RV}{\chi_\phi} + \frac{R\tau_{rs}}{\chi_\phi l} \qquad (2)$$

In eq.(2), χ_i is the ion heat diffusivity, which is determined from the local power balance. The left hand side term is obtained from CXRS measurements, while the term between brackets, the normalized net dimensionless torque, hereafter abbreviated as t_i^*-Γ_N^*, is obtained from a combination of measurements and calculations. The particle flux term in (2) is a small (~10%) correction to the gross torque from the NBI. The form of eq.(2) lends itself to determining the Prandtl number χ_ϕ/χ_i and the non-diffusive contributions, as well as their parameter dependencies, by means of regressions. We should point out here already, that attempts to separate the pinch from residual stress effects by means of regressions have not led to compelling results. The normalization of $\nabla\omega$ to ω, is unproblematic for our dataset, because even the lowest values of ω, at r/a $\approx$ 0.85, are still close to 40% of the core values, because of the large edge rotation pedestal in H-mode.

As only steady-state conditions established for well over 1 second, i.e. longer than both the energy confinement time and the fast ion slowing down time, are included in the database, there is no need to distinguish between the collisional torque due to passing beam ions and the instantaneous torque due to trapped beam ions, although both are included. The ion heat flux Q_{iNB} [W/m^2] from the neutral beams and the torque surface density t were evaluated using a beam deposition code which does not take into account ion orbit effects. A small correction was applied to Q_{iNB} and t to bring these into line with more accurate calculations, effected for a small subset, using the ASCOT Monte Carlo orbit following code [17]. As an accurate determination of the power balance is necessary for evaluating χ_i, we restricted the data to those where the equipartition flux Q_{ei}, which is subject to fairly large uncertainties, is smaller in magnitude than $0.35Q_i$, where $Q_i = Q_{iNB} + Q_{ei}$ is the total ion heat flux. Despite this restriction, the data cover a wide range in dimensionless parameter space, as shown in table 1.

As most of these plasmas are strongly rotating due to the external momentum input by NBI, the ordering parameter [8] $\rho_i^*(R/L_{Ti})^2/u$ is in the range 0.04-1 for 98% of the 944 samples in the database and below 0.5 for 90% of the samples. This indicates, according to theory [8], that the pinch, rather than residual stresses, is the most important non-diffusive transport mechanism in these plasmas. Approximately half of the samples the database include Ion Cyclotron Resonance Heating

(ICRH), providing up to 40% of the total heating power, using the hydrogen minority resonance scheme, which mainly provides electron heating. JET plasmas heated only with H-minority ICRH have rotation frequencies one order of magnitude below those of NBI heated discharges [18,19], much of which may be due to residual stresses. The gradients are evaluated in the equatorial plane as averages of the high and low field side local gradients, following a tensioned spline fit over the profile data. As the trapped particle fraction, $f_t \approx \varepsilon^{1/2}$, is an important physics parameter for momentum transport [9], all profiles were re-mapped, using ε as the radial coordinate and sampled for 7 positions between $\varepsilon = 0.075$ and 0.255.

Figure 1 shows simple regressions for two positions, $\varepsilon = 0.165$ and $\varepsilon = 0.255$, aimed at determining only the typical Prandtl number and the non-diffusive term. The symbols are resolved by the confinement factor H98, showing that the relationship between the net dimensionless torque and R/L_ω does not depend on confinement quality.

The regressions in fig.1 are part of a profile, shown in fig.2, constituted of 7 partly overlapping intervals, over which gradients were evaluated. Since we cannot rule out a residual stress contribution based solely on the experimental data, we lump the pinch and the residual stress terms together as $RV/\chi_\phi + \tau_{rs}^*/u$, where $\tau_{rs}^* = \tau_{rs}/(m_i n_i v_i \chi_\phi)$ is a dimensionless residual stress number. The last closed flux surface is typically at ε=0.3. The figure shows that while the Prandtl number is close to unity, without a significant radial dependence, the non diffusive part has a clear radial dependence. The vertical bars indicate the 90% confidence intervals for the regressions. Not applying the above mentioned orbit effect corrections, or excluding all shots with ICRH, does not lead to any significant changes in the non-diffusive terms evaluated from the regressions.

The magnitude of the pinch is consistent with the one obtained in NBI modulation experiments [2,3]. Toroidal field ripple scan experiments, in the range 0-1%, have also provided corroborating evidence [20]. The ion losses caused by the ripple produce an edge torque in the counter-I_p direction, which can be of similar magnitude as the NBI torque, allowing a scan of the torque without significantly altering other plasma parameters. These experiments were consistent with $P_r \approx 1$ and a pinch RV/χ_ϕ rising from near 2 for $\varepsilon = 0.1$ to near 8 for $\varepsilon = 0.3$.

The database approach allows the investigation of multiple parameter dependencies for the first time, by testing hundreds of parameter combinations More than one fit of similar quality can be obtained with different parameter combinations, as a result of correlations in the database. Combinations including t_i^*-Γ_N^*, R/L_n, q, ε, T_i/T_e, s, and R/L_{Ti} or R/L_{Te} provide the best regressions. The torque t_i^*-Γ_N^* and R/L_{Ti} are strongly correlated and cannot be meaningfully used in the same regression. In fig.3, we present the 5 parameter fit (not including R/L_{Ti}) over 3000 data points with the lowest standard deviation ($\sigma = 1.29$):

$$R/L_\omega \approx 1.2(\pm 0.1)(t_i^*\text{-}\Gamma_N^*) + 0.41(\pm 0.07)R/L_n + 12(\pm 1.4)\varepsilon^{1/2} + 0.41q(\pm 0.12) - 1.9(\pm 0.68)T_i/T_e - 1.7(\pm 0.9) \quad (3)$$

The brackets refer to 90% confidence intervals. The first RHS term is the diffusive term and the remaining terms can be interpreted as representing the parameter dependencies of the non-diffusive

transport terms. Statistically, the diffusive term accounts for some 52% of overall variation of $R/L_{\omega'}$ followed by $\varepsilon^{1/2}$ (28%), R/L_n (20%) and q (9%) and T_i/T_e (8%). Since all parameters are correlated with the radial variable ε, we have also performed regressions for fixed values of ε. These confirm the importance R/L_n q (and/or s) and T_i/T_e for non-diffusive momentum transport. We used neural network based regressions to assess to which extent the imposed linear functional forms limit the quality of the fits. The best neural network based regressions using the same variables perform only slightly better ($\sigma \approx 1.2$) than the linear regressions, showing that the latter do capture the most important dependencies.

To compare the parametric dependencies obtained in the experiments to the theoretical predictions, a representative subset of 420 samples of the database representative of the same dimensionless parameter domain as the entire experimental dataset was used as input for a series of linear gyrokinetic calculations performed with the *δf* flux-tube code GKW [21]. The calculations were performed for two representative wave vectors, $k_\theta\rho_i = 0.15$ *and* 0.45. The latter corresponds to the typical value at which the growth rate maximises in linear simulations and the former to the maximum flux in non-linear simulations. Circular geometry, electrostatic fluctuations and two kinetic species (deuterons and electrons) were assumed. The simulations were performed without background $E\times B$ shear flow, as its contribution to the momentum flux is negligible in the high flow regime [8] and did not include any other residual stress contributions. The dominant instability was identified to be the Ion Temperature Gradient mode (ITG).

For each input parameter combination, two calculations were performed. The first of these, with $u = 0.1$ and $u' = uR/L_\omega = 0$ provided the momentum pinch part, while the second, with $u = 0$ and $u' = 1$ provided the diagonal (diffusive) part. The Prandtl and pinch numbers were then deduced from the fluxes obtained in each case as described in ref.[22]. Collisional and non-collisional calculations mostly produce similar results. A few additional simulations were performed with the full MHD equilibrium, confirming that the up-down asymmetry residual stress [12] is negligible in the core of these plasmas and that the circular flux surfaces assumption provides, within 15%, similar Prandtl and pinch numbers, and barely affects their parametric dependencies. The choice of linear simulations for this statistical comparison is mainly dictated by practical reasons, however, it is also supported by the fact that the dominant parametric dependencies of the pinch number are largely similar in linear [9] and non-linear calculations [8]. In fig.4, we see that the predicted pinch number and Prandtl numbers at $k_\theta\rho_i = 0.15$ *and* 0.45 are of the same magnitude as the experimental results in fig.2 and more importantly, that the radial dependence of the pinch number is well reproduced. A more detailed comparison would require a suitable spectral average over the entire unstable domain (typically $0.05 < k_\theta\rho_i < 1.5$), as introduced for instance in the TGLF quasi-linear momentum transport model [23], or even much more laborious non-linear calculations. The linear calculations at $k_\theta\rho_i = 0.15$ and 0.45 however provide a rather good proxy of the non-linear results. A sample-by-sample comparison, shown in fig.5, using for simplicity the average Prandtl and pinch numbers from the GKW calculations, shows a fair agreement of theoretically expected and observed $R/L_{\omega'}$

The predicted values are about 70% of the experimentally inferred non-diffusive terms, supporting the prediction that they are dominated by the Coriolis pinch. The main parameter dependencies are also similar. The best 5 parameter regression for the average theoretical pinch is obtained, with $\rho_i = 0.35$, as

$$RV/\chi_\phi \approx 0.44(\pm 0.35)R/L_n + 7.7(\pm 1.5)\varepsilon^{1/2} + 0.39(\pm 0.06)\, q - 0.1(\pm 0.02)R/L_{Te} - 0.15(\pm 0.12)s - 4.3 \pm 0.6 \quad (4)$$

The first three of these parameters match three of those representing the non-diffusive terms in eq.(3), with similar coefficients, further supporting the identification of the observed non-diffusive transport as being due largely to the Coriolis pinch. However the 30% difference and e.g. the presence of the T_i/T_e dependence in the experimental data, which is not seen in the theoretical pinch, leave the door open for significant contributions from other processes, such as from residual stresses. Residual stresses are the subject of further investigations.

We wish to warn that scaling relations such as eq.(3) & (4), although popular, remain subject to data correlation issues and ultimately fail to capture the complex and non-linear dependencies of the transport coefficients on the input parameters. Correlations are however not an impediment for empirical predictions, as long as the parameter space, which predictions are sought for, is similarly correlated. This is largely the case for ITER, with the important exception of ρ_i^*. The fact that ρ_i^* only appears with low statistical significance and relevance, if at all, in our regressions, and the absence of a theoretical dependence of the Coriolis pinch on this parameter, suggest that our empirical and our theory-based scalings for the momentum pinch may also hold for ITER.

To summarise, the experimental results show that non-diffusive momentum transport processes are ubiquitous throughout the JET H-mode and hybrid regime database. Moreover, the experimental dependencies for R/L_ω and the theoretical pinch number RV_ϕ/χ_ϕ from linear GKW calculations for the Coriolis pinch share three of their most relevant parameter dependencies, i.e, those on R/L_n, q and ε. Overall, the predicted pinch amounts to approximately 70% of the observed non-diffusive momentum transport. Hence, while our experimental results are supportive of the theoretical prediction [8] that the Coriolis pinch is the most important non-diffusive momentum transport mechanism in NBI-driven rotating tokamak plasmas, such as those of H-modes and hybrid regimes in JET, they do not rule out that other processes, such as residual stresses, may also play a role.

ACKNOWLEDGMENT

This work was supported by EURATOM and carried out within the framework of the European Fusion Development Agreement. The views and opinions expressed herein do not necessarily reflect those of the European Commission.

REFERENCES

[1]. J.E. Rice, Nuclear Fusion **47**, 1618 (2007)

[2]. T. Tala et al, Physical Review Letters **102**, 075001 (2009)

[3]. T. Tala et al, Nuclear Fusion 123002 **51** (2011)
[4]. A. Bortolon et al, Physical Review Letters **97**, 235003 (2006)
[5]. R.M. McDermott, Plasma Physics and Controlled Fusion **53**, 035007 (2011)
[6]. S.H. Müller et al, Physical Review Letters **106**, 115001 (2011)
[7]. W.M. Solomon et al, Nuclear Fusion **51** (2011) 07301
[8]. A.G. Peeters et al, Nuclear Fusion, **51**, 094027 (2011)
[9]. A.G. Peeters et al, Physical Review Letters **98** 265003 (2007)
[10]. T.S. Hahm et al, Physics of Plasmas **14**, 072302 (2007)
[11]. A. G. Peeters et al, Physics of Plasmas **16**, 062311 (2009)
[12]. Y. Camenen et al, Physical Review Letters **102**, 125001 (2009)
[13]. F. Romanelli and R. Kamendje, Nuclear Fusion **49**, 104006 (2009)
[14]. Joffrin E. et al. in Fusion Energy 2010 (Proc. 23rd Int. Conf. Daejeon, 2010) (Vienna: IAEA) CD-ROM file [EX/1-1 and http://www-naweb.iaea.org/napc/physics/FEC/FEC2010/html/index.htm]
[15]. E.J. Doyle et al. Progress in the ITER Physics Basis Chapter 2: Plasma confinement and transport 2007 Nuclear Fusion **47** S18
[16]. M Shimada et al. Progress in the ITER Physics Basis Chapter 1: Overview and summary 2007 Nuclear Fusion **47** S1
[17]. J.A. Heikkinen *et al*., Journal of Computational Physics **173**, 527 (2001)
[18]. M.F.F. Nave et al, "JET intrinsic rotation studies in plasmas with a high normalised beta and varying toroidal field ripple", to be published in Plasma Physics and Controlled Fusion, special issue "JET Task Force H 2011", March 2012
[19]. J.-M. Noterdaeme et al, Nuclear Fusion **43** (2003) 274
[20]. T.W. Versloot, Ph.D thesis, Eindhoven University of Technology, The Netherlands (2011)
[21]. A.G. Peeters et al. Computer Physics Communications, **180**, 2650 (2009)
[22]. Y. Camenen et al., Nuclear Fusion **51**, 073039 (2011)
[23]. G.M. Staebler et al., Physics of Plasmas **18**, 056106 (2011)

	$\lvert t_i^* - \Gamma_N^* \rvert$	u	R/L_ω	R/L_n	R/L_{Ti}	R/L_{Te}	T_i/T_e	ε	ν_{eff}	β	ρ_i^*	q	s
min	0.05	0.05	0.4	1	3	3	0.6	0.075	0.06	0.001	0.002	0.9	0.01
max	14	0.38	24	10	19	17	2.7	0.255	5.2	0.049	0.01	4.6	10

Table 1: Dimensionless parameter ranges in JETPEAK H-mode and hybrid database. Here $u = R\omega/v_i = R\omega/(2T_i/m_i)^{1/2}$ *is the Mach number,* $L_\omega = \omega/\nabla\omega$ *etc,* $\varepsilon = r/R$ *is the inverse aspect ratio,* $\nu_{eff} = 10^{-14} R Z_{eff} n_e T_e^{-2}$ *is the normalised collisionality,* β *is the local thermal plasma pressure normalised to the magnetic pressure,* ρ_i^* *is the thermal ion Larmor radius normalised to R, q is the local safety factor obtained using the equilibrium code EFIT and* $s = \varepsilon R/L_q$.

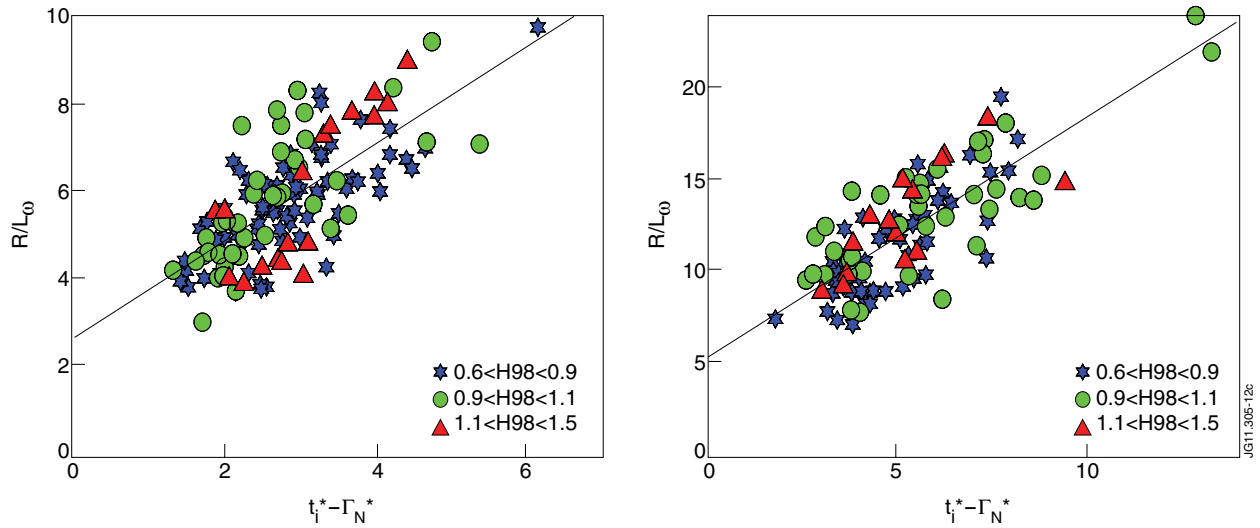

Figure 1: Normalized rotation frequency gradient versus net dimensionless torque, showing a diffusive component (slope) and a non-diffusive component (intercept a zero effective torque) for $\varepsilon \approx 0.165$ ($r/a \approx 0.45$, left) and $\varepsilon \approx 0.255$ ($r/a \approx 0.85$, right). The symbols refer to the IPB98(y,2) confinement factor.

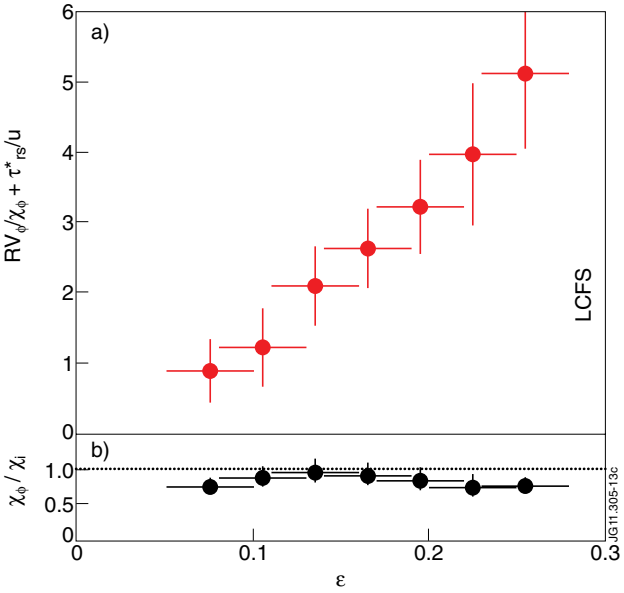

Figure 2: Profiles of average pinch number (a) and Prandtl number (b) for seven radial intervals.

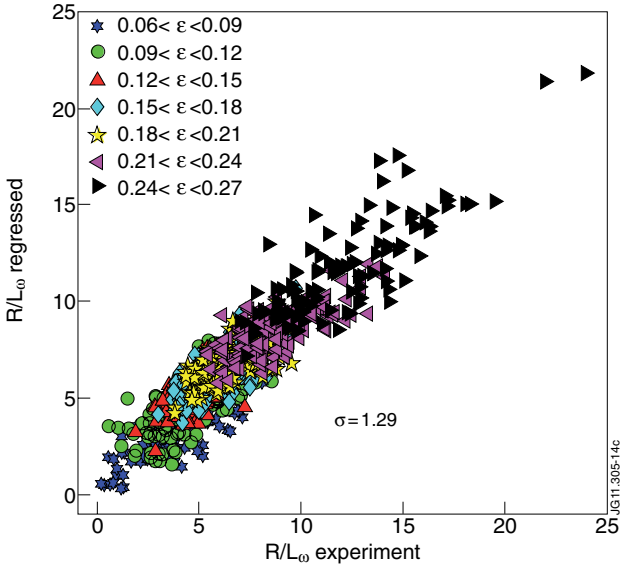

Figure 3: Regression corresponding to eq.(3). The symbols correspond to the same values of ε as in figure 2.

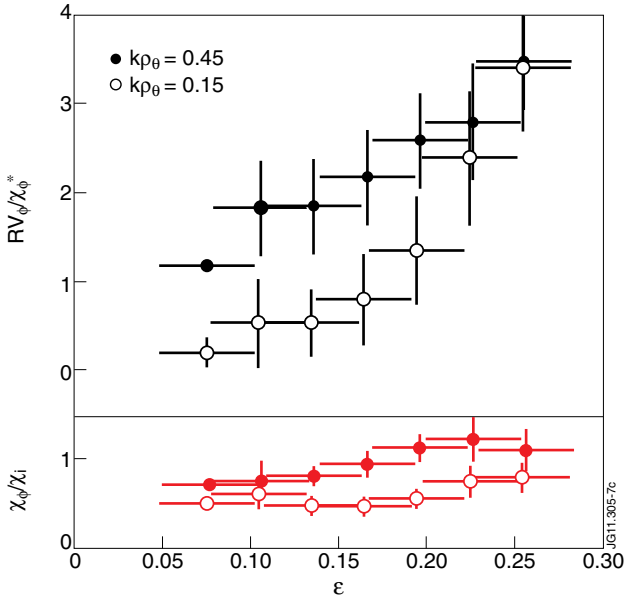

Figure 4: Average and standard deviation (bars) of Prandt (red) and pinch numbers (black) from GKW, for two different wavenumbers.

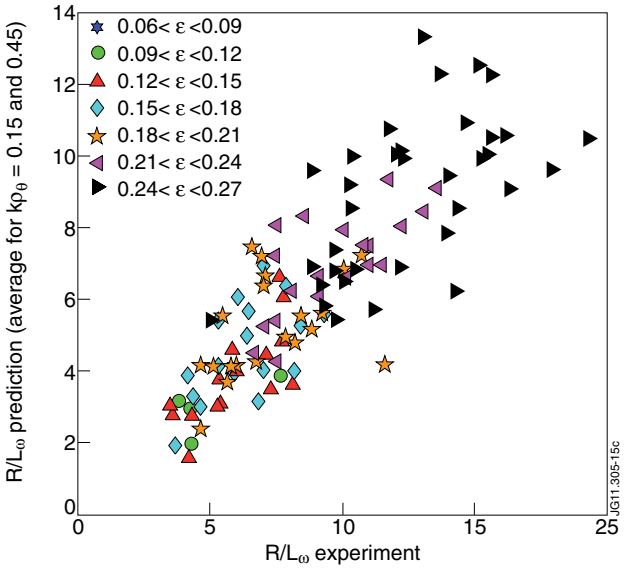

Figure 5: Sample-by-sample comparison of experimental and modeled R/L_ω.